Science Bulletin xxx (xxxx) xxx

Contents lists available at ScienceDirect

Science Bulletin

journal homepage: www.elsevier.com/locate/scib

Article

Scaling dictates the decoder structure

Jingxiang Shen [a], Feng Liu [a,b], Chao Tang [a,b,c,*]

[a] Center for Quantitative Biology, Peking University, Beijing 100871, China
[b] School of Physics, Peking University, Beijing 100871, China
[c] Peking-Tsinghua Center for Life Sciences, Peking University, Beijing 100871, China

ARTICLE INFO

Article history:
Received 16 March 2022
Received in revised form 6 May 2022
Accepted 13 June 2022
Available online xxxx

Keywords:
Scaling
Pattern formation
Drosophila gap gene
Morphogen gradient
Phenomenological decoder

ABSTRACT

Despite fluctuations in embryo size within a species, the spatial gene expression pattern and hence the embryonic structure can nonetheless maintain the correct proportion to the embryo size. This is known as the scaling phenomenon. For morphogen-induced patterning of gene expression, the positional information encoded in the local morphogen concentrations is decoded by the downstream genetic network (the decoder). In this paper, we show that the requirement of scaling sets severe constraints on the geometric structure of such a local decoder, which in turn enables deduction of mutants' behavior and extraction of regulation information without going into any molecular details. We demonstrate that the *Drosophila* gap gene system achieves scaling in the way consistent with our theory—the decoder geometry required by scaling correctly accounts for the observed gap gene expression pattern in nearly all maternal morphogen mutants. Furthermore, the regulation logic and the coding/decoding strategy of the gap gene system can also be revealed from the decoder geometry. Our work provides a general theoretical framework for a large class of problems where scaling output is achieved by non-scaling inputs and a local decoder, as well as a unified understanding of scaling, mutants' behavior, and gene regulation for the *Drosophila* gap gene system.

1. Introduction

In embryonic development, a cell must know its position in space in order to determine its fate. In the early embryo of *Drosophila* and many other cases, this positional information is encoded in a space-dependent signal like morphogen gradient [1–3]. The decoder in the cell (usually a gene network) reads the local value of the signal to infer the cell's spatial position and express the appropriate genes, as exemplified in the French-flag model [1,4,5].

The physiological functions of most animals are based on their accurate body structures, which are built by embryogenesis. Embryogenesis is under precise genetical regulation in general, but the overall embryo size is usually not. In long germ-band insects like the *Drosophila*, the size of the early embryo is equal to the egg size, which is strongly affected by environmental conditions such as temperature [6], oxygen level [7], etc. Therefore, the developmental program must be properly designed to ensure individuals of the same species develop in the same correct proportion regardless of the overall size change. Such scaling property is very common in development [8–12] and especially so for *Drosophila* [13–15].

However, for gene patterning guided by morphogens, scaling does not come by itself. A morphogen gradient is formed via diffusion and degradation. It has a decay length determined by the diffusion constant and the degradation rate, which are usually fixed independent of the embryo size. One solution is to introduce additional regulations to make the morphogen gradient scale by itself, i.e., being able to adjust its decay length according to the embryo size. This kind of strategy is adopted by systems like the *Xenopus* germ-layer specification [16,17] and the *Drosophila* wing disc [18–20] and dorsoventral axis patterning [21]. For the *Drosophila* anterior-posterior (A-P) segmentation studied here, much effort has been devoted to measuring the scaling property of the key morphogen Bicoid (Bcd) [22–25], but the results indicate that it should have a fixed decay length instead of a scaling one.

Downstream of the maternal morphogens, the gap genes are the first set of *Drosophila* A-P segmentation genes, whose expression pattern appears to scale with the embryo length almost perfectly. Evidence of scaling gap gene pattern is reported in wild-type (WT) embryos with natural length fluctuations [22], as well as in artificially selected fly lines with much larger and smaller embryos [26]. In a recent experiment, the expression domains of all four trunk gap genes (*hunchback* (*hb*), *Krüppel* (*Kr*), *knirps* (*kni*), and

* Corresponding author.
E-mail address: tangc@pku.edu.cn (C. Tang).

https://doi.org/10.1016/j.scib.2022.06.014
2095-9273/

giant (*gt*)) show scaling boundary positions even when embryo length is artificially reduced by 30% [25]. Although those results might not be sufficient to imply perfect scaling—the measured scaling error is less than 3% of embryo length [13–15], still larger than the baseline noise in embryos of identical size [27,28], we believe that this < 3% accuracy is enough to confirm the presence of scaling mechanism in the gap gene system, since the "null hypothesis" that gap gene simply follow the Bcd thresholds should give a scaling error of at least 10%. Therefore, although subsequent refinements and repair mechanisms may exist by regulating tissue growth and cell death at later stages of development [29–31], a scaling blueprint of the future body plan is laid down at the blastoderm stage by the gap genes, by reading the non-scaling maternal morphogens.

There are many proposed mechanisms attempting to solve the gap genes scaling problem, e.g., amplitude correction or "partial scaling" of the morphogen (Bcd) gradient [24,32,33], decoding unsteady Bcd gradient [34,35], the dynamical "canalization" of the gap gene network [36], and positional error correction based on diffusion of the gap gene products [37]. These studies provided much data and insights. Nonetheless, a comprehensive understanding that correctly accounts for scaling throughout the entire embryo is still lacking, as well as predictions that can be validated systematically and experimentally.

Another valuable early idea is the bi-gradient model [1,38,39] — if a second posterior gradient is present in addition to the anterior Bcd gradient, a cell can in principle have enough information to "compute" its relative position in the embryo. For historical reasons, the bi-gradient model is not well-developed and remains largely a theoretical possibility for the gap gene case (see Supplemental Text S1 online), though this idea that integrative decoding of two opposing gradients has been successfully applied to vertebrate neural tube development in a later work [40].

The bi-gradient model represents the idea of "local decoder", i.e., the cell fate at each spatial position is a function of morphogen levels at this spatial point *alone*. The developmental gene regulation network is effectively a decoder, working in a spatially decoupled manner, mapping a combination of local morphogen concentrations to a local cell fate. This decoding idea has also been widely adopted in analyzing optimal extraction of positional information from single or multiple noisy morphogen gradients [40–44]. Such a "local decoding" framework is the minimum decoding scheme since it needs no cell–cell signaling at the decoding stage. This is of particular interest for the gap gene system, since at this developmental stage the embryo is a syncytium without well-separated cells.

Measuring the morphogen gradients and WT gap gene patterns to such a precision that can directly prove or disprove the above-mentioned theoretical models is extremely challenging. This makes the gap gene scaling problem remains to be settled—i.e., scaling or non-scaling morphogen, local or non-local decoding, etc. In this paper, we approach this problem in a different way. By starting from the simplest assumption that scaling here is achieved with non-scaling maternal morphogens and a local decoder, we show that the necessary and sufficient condition to generate a scaling gene expression pattern across the entire embryo contains rich information on the geometric structure of the decoder, i.e., the decoder structure is dictated purely from its function (scaling). Then, the bulk of the existing experiments on morphogen mutants can be employed in the study of scaling—in our framework it is just the same decoder applied to altered inputs. The measured mutants' patterns are in excellent agreement with the prediction by the scaling local decoder, which strongly supports our stating assumption that scaling of the *Drosophila* gap gene system should originate from localized integrative decoding of the multiple non-scaling input gradients.

2. Results

2.1. The geometric structure of the decoder is determined by the scaling requirement

We first illustrate our basic idea using a bi-gradient model [1,38,39], and demonstrate how the local decoder is dictated directly by the scaling requirement. In this simplified model, there are two opposing non-scaling morphogens, M_1 and M_2, having exponentially shaped gradients with a fixed length constant λ (Fig. 1a). In an embryo of length L, the two gradients read:

$$M_1 = e^{-x/\lambda}, M_2 = e^{-(L-x)/\lambda}, (0 < x < L). \quad (1)$$

Here, the length of a standard-sized embryo is used as the length unit. Define the relative coordinate $y \equiv x/L$, so that the larger ($L > 1$) and the smaller ($L < 1$) embryos can all be placed together with the standard-sized embryos ($L = 1$) for comparison. Obviously, the morphogen gradients with fixed length constant (Eq. (1)) are not scaling by themselves since they depend not only on the scaled coordinate y but also on the length L (Fig. 1b),

$$M_1 = e^{-yL/\lambda}, M_2 = e^{-(1-y)L/\lambda}, (0 < y < 1). \quad (2)$$

Consider for example the position $y = 0.35$ as the boundary separating two different cell fates in the embryo. In a smaller embryo, as the absolute distance to both termini is shorter at this position, local levels of both morphogens are higher, and vice versa. When L varies, the $y = 0.35$ point traces out a line on the M_1–M_2 plane (Fig. 1c). Therefore, for a local decoder to give perfect scaling outputs, this y-constant line must be followed by the decision boundary of the decoder, which maps an (M_1, M_2) pair to a gene expression state ("fate"). In other words, the requirement imposed by scaling is enough to determine the effective input–output relation (coloring scheme) of the decoder in this double-gradient case, no matter how the decoder is implemented biochemically. The cell fate can also be represented by its equivalent position in WT, denoted as $\tilde{y}$. In this case:

$$\tilde{y}(M_1, M_2) = \frac{\ln M_1}{\ln M_1 M_2}, \quad (3)$$

which is obtained by eliminating L from Eq. (2).

Once determined by its scale-invariant performance in WT embryos, the same decoder (Eq. (3)) can be applied to mutant embryos where the maternal morphogen profiles are perturbed but the decoding machines are intact. In the case considered here, along the A-P axis of a WT embryo of size L, the local concentrations of the two morphogens fall on the hyperbolic curve $M_1 M_2 = e^{-L/\lambda}$ (according to Eq.(2)). On the other hand, consider a standard-sized ($L = 1$) mutant embryo where the M_1 copy number is doubled:

$$M_1 = 2e^{-y_{mut}/\lambda}, \; M_2 = e^{-(1-y_{mut})/\lambda} \quad (4)$$

This mutant is also represented by a hyperbolic curve $M_1 M_2 = 2e^{-1/\lambda}$(Fig. 1d). Note that this curve is exactly the one describing a WT embryo of size $L = 1 - \lambda \ln 2$ though points of the same cell fate locate at different y's in WT and the mutant. For example, the blue-green boundary at $y = 0.35$ in WT is shifted to 0.46 in the mutant.

In general, for any y_{mut} in this mutant embryo, there always exists a corresponding position y_{WT} in a (non-standard-sized) WT embryo with exactly the same morphogen values, hence the same cell fate $\tilde{y}$. In this case, substituting the mutant's morphogen profile (Eq. (4)) into the decoder function (Eq. (3)) yields such a mapping:

$$y_{WT}(y_{mut}) \equiv \tilde{y}(y_{mut}) = \frac{y_{mut} - \lambda \ln 2}{1 - \lambda \ln 2}. \quad (5)$$

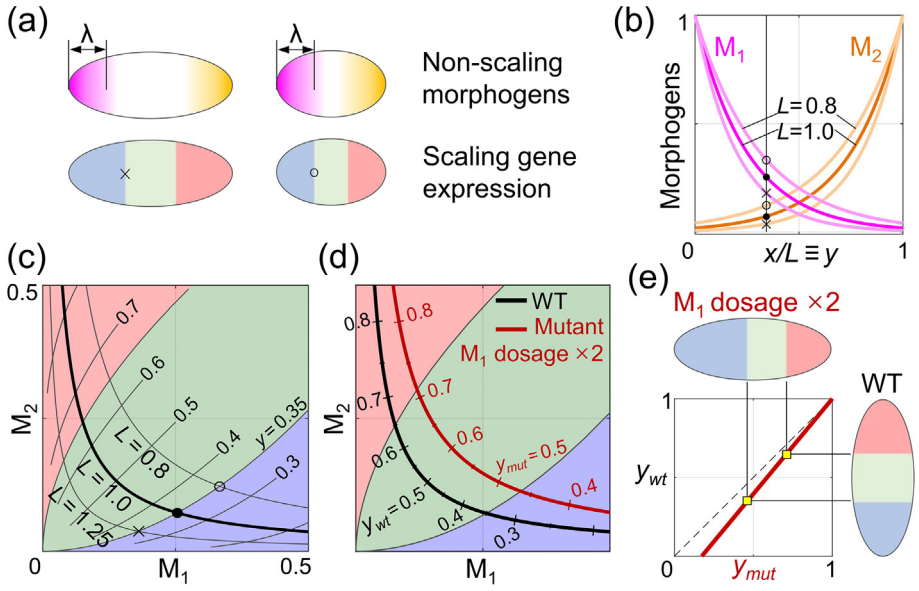

Fig. 1. Generating scaling output by reading the local values of two non-scaling gradients. (a) A schematic sketch with two embryos of different sizes. The two morphogen gradients are shown in the upper panel and the desired scaling output patterns are shown below. (b) The same relative position $y \equiv x/L = 0.35$ has a higher level of both morphogens in a smaller embryo (marked by "O") than in a larger one ("X"). Situations where $L = 0.8$, 1.0, and 1.25 are shown here. (c) In the M_1–M_2 space, the standard-sized WT embryo is represented by the black curve. As L varies, the $y = 0.35$ point traces out a line, which overlaps with the blue-green decision boundary of the ideal scaling decoder. (d) Maternal morphogen profiles in a mutant are also represented by a curve in the M_1-M_2 space. The red curve stands for an $L = 1$ embryo where the M_1 dosage is doubled. The corresponding cell fates along this red curve, hence along the A-P axis of this mutant, can be directly read out. (e) The predicted "fate map" of the mutant in (d). All gene expression boundaries, if their positions in WT were plotted against their shifted positions in the mutant, should lie on the fate map.

We call this mapping $\tilde{y}(y_{\mathrm{mut}})$ the "fate-map" of this mutant. This fate map can be tested experimentally by plotting the measured positions of y_{mut} against y_{WT} for each given cell fate—for example, each expression domain boundary (Fig. 1e). If the measured boundary positions in mutants match the scaling predictions, then it would strongly support that the underlying gene network decodes the multiple morphogens in such a specific way that enables scaling. For a local decoder, scaling and mutants' behavior are just different aspects of the same underlying decoder geometry. In the following sections, we demonstrate that the *Drosophila* gap gene system is indeed a decoder of this kind.

2.2. Construction of a phenomenological decoder for Drosophila

Following the procedure outlined above, we next construct a decoder for the *Drosophila* gap gene system, using all the three maternal morphogen gradients Bcd, Nanos (Nos), and Torso (Tor). These three are also the only upstream-most gradients [45], since $bcd^{-}nos^{-}tor^{-}$ triple mutant shows spatially uniform gap gene expression [43,46]. Other gradients (like Caudal) are known to be derived from these three primary morphogens, and thus should not be considered explicitly.

Experimental measurements suggest that Bcd has a fixed length constant [13,22,24,25] and an overall amplitude positively correlated with embryo length [24,32,33]. So, it is modeled as:

$$\mathrm{Bcd}\,(y, L) = L^{\beta} e^{-yL/\lambda_B}. \tag{6a}$$

It is evident from Eq. (6a) that there is a special point $y = \beta\lambda_B$ where the Bcd level is L-independent owning to the amplitude correction. Some previous studies claimed that this effect makes Bcd a "partial scaling" gradient, and may be the main reason for gap gene scaling [24,26]. Although we do not agree with this explanation in general, as it cannot account for scaling throughout the entire embryo especially in the head and abdomen regions far away from the $y = \beta\lambda_B$ point [14,15,25,26], this amplitude factor has been verified experimentally, thus should be considered here if we wish to model the real situation in *Drosophila* (Fig. S1 online).

The *Drosophila* posterior gradient Nos has an exponential profile fixed to the posterior. Based on the existing knowledge that it is also formed through localized synthesis and diffusion [2,45], a reasonable assumption is that it takes the same non-scaling form as M_2 in Fig. 1. It is well known that Nos functions solely through repressing the maternal component of the gap gene product Hb (mHb) in the posterior half of the embryo [47–49]. Therefore, the "immediate" posterior morphogen should be mHb. If the inhibition of mHb by Nos is modeled by an inhibitory Hill function, then the mHb gradient should take a sigmoidal shape (Fig. S2 and Supplemental Text S2 online):

$$\mathrm{mHb}(y) = \mathrm{mHb}_0/\left(1 + e^{\alpha L(y-1+(1-\lambda_H)/L)}\right). \tag{6b}$$

The source of Tor activity locates at both termini of the embryo and extends spatially through diffusion [50,51]. By minimal assumptions, we take a fixed length constant for its profile, too.

$$\mathrm{Tor}(y) = e^{-yL/\lambda_T} + e^{-(1-y)L/\lambda_T}. \tag{6c}$$

All parameters above are fitted from published experimental data [24,25,47–49,52,53] (see Supplemental Text S2 online for details). Taken together, in parallel with Eq. (2), Eq. (6) gives a complete description of the *Drosophila* morphogens responsible for A-P patterning, as shown in Fig. 2a.

Downstream of the maternal morphogens, the gap genes (*hb*, *Kr*, *kni*, and *gt*) are the first to display a scaling pattern [22,26]. The *Drosophila* embryo has around 100 rows of cells along the A-P axis before gastrulation. Nearly any two of them can be distinguished by their gap gene expression [28], so there are effectively around 100 different cell fates along the A-P axis and the fate map $\tilde{y}$ should be discussed at the resolution of 0.01. To visualize these cell fates by colors, we group them into 8 classes according to the dominantly expressing gap gene (Fig. 2b).

A standard-sized ($L = 1$) WT embryo is represented by a 1-d curve in the space of (Bcd, mHb, and Tor). When L varies, this curve

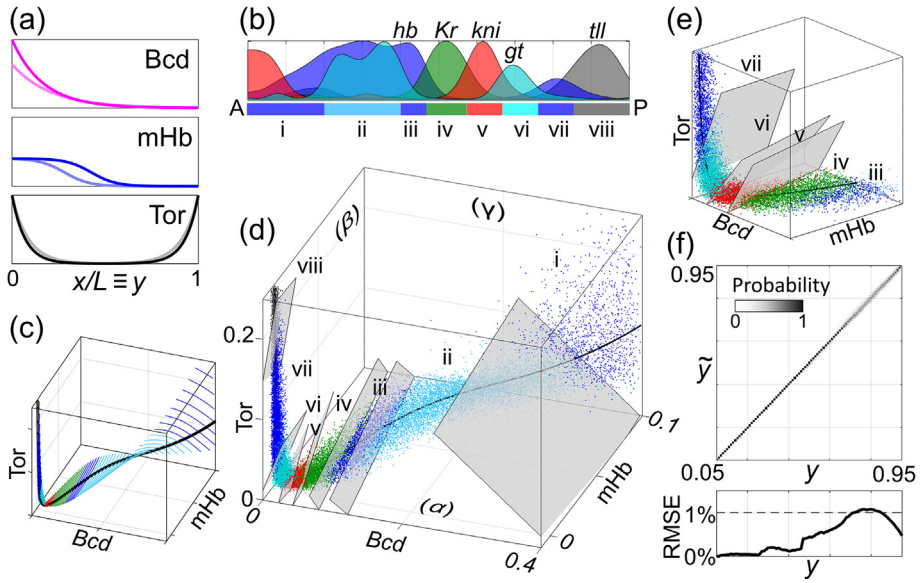

Fig. 2. The phenomenological scaling decoder for *Drosophila* A-P patterning. (a) The three non-scaling maternal gradients in the relative coordinate $y \equiv x/L$ (Eq. (6)). The morphogen profiles for a standard size WT embryo ($L = 1$, darker lines) and a smaller one ($L = 0.8$, lighter lines) are shown. (b) 101 different cell fates along the A–P axis are grouped into 8 domains according to the gap gene expression. The normalized gap gene profiles are adopted from Ref. [27] and a Gaussian smoothing is applied. (c) In the (Bcd, mHb, and Tor) space, the standard-sized WT embryo is represented by the black curve along which y varies from 0 to 1. When L changes, each point on this curve traces out a line representing the morphogen values at this y position in WT embryos of different sizes. Only the region corresponding to $L = 0.8$–1.2 are plotted here. The y-constant lines shown there have spacing $\Delta y = 0.01$ along the A–P axis. (d) Poisson noise is added to the morphogen levels and the embryo length is sampled from a normal distribution, turning the 2-d WT surface in (c) to a 3-d distribution of WT data points. The optimal decision boundaries can be well approximated by a set of linear planes. (e) A magnification of (d). The iv–v, v–vi, and vi–vii boundary planes are shown. (f) Positions decoded from the morphogen values ($\tilde{y}$) vs. the ground truth (y) for the WT data points in (d). Since gap gene expression is affected by the Dorsal–Ventral system when being very close to embryo termini, we only discuss y between 0.05 and 0.95 hereafter. The root-mean-square-error (RMSE) is hardly larger than 1%.

sweeps out a 2-d WT surface. Following our arguments in Fig. 1, the ideal output of a scaling decoder on this WT surface can be immediately determined—lines of constant y values should have the same cell fate (Fig. 2c).

In reality, *Drosophila melanogaster* embryo length varies approximately between 450 and 570 μm ($\sim \pm$ 10%) across different fly stocks [14], while scaling for the peaks and boundaries of the gap gene expression is near perfect at least to the resolution of currently available measurements [13,15]. To have a more realistic picture, we hereafter sample L from a normal distribution $L \sim N(\mu = 1, \sigma = 0.1)$ to simulate the effects of length fluctuation across *Drosophila melanogaster* stocks. Another important aspect is noise in morphogen profiles. When morphogen level approaches zero it should have huge relative noise and thus cannot carry useful information. Also, there is embryo-to-embryo variability in morphogen amplitude. We introduce explicitly Poisson noise terms to the morphogen values to reflect that the gradients themselves are noisy (Supplemental Text S3 online). The amplitude of such noise is selected to reflect the experimentally observed variations. For example, Bcd is the most extensively studied gradient, whose positional error at each spatial position has been carefully measured [54]. Our Poisson noise term is then selected to introduce a positional error of the same order (Fig. S3 online). As a result, the "colored lines" (i.e., ideal decoder output) in Fig. 2c now transform into more realistic 3-d distribution as in Fig. 2d.

The gap gene network (the decoder) should be able to classify all the points in Fig. 2d into classes (real cell fate) that matches their colors. In a sense, this is an "optimal decoding" problem in the presence of noise [28,40,41,43]. Here, the dominant source of noise is the embryo length variation and the main goal is to preserve scaling.

Besides just obtaining a decoder that performs such classification tasks (like a Bayesian one discussed in Supplemental Text S4 online), we are more interested in figuring out the shape of those decision boundaries explicitly. The complexity and nonlinearity of the decision boundaries are directly related to whether they can be satisfactorily approximated by a gene regulation network, as will be discussed later. Here comes an important observation, that for the *Drosophila* case the boundaries between regions of different desired outputs (colors) are effectively linear—any local decoder that achieves scaling must effectively behave like a set of linear classifiers, at least within the region covered by the WT data points. Therefore, we fit the phenomenological decision boundaries with planes (see Supplemental Text S5 online for details). Points of different colors seem to be separated satisfactorily in this way (Fig. 2d, e, and Fig. S4d online).

The three maternal gradients can not only determine boundaries of gap gene expression domains, but also ~100 distinct A–P cell fates as mentioned above. Thus, we can construct a (approximately) continuous version of the decoding function using more linear classifiers of this kind. Along the A–P axis, we fit 100 such classification planes at 100 equally spaced y positions (Supplemental Text S5 online). The linear classifiers work sufficiently well with the decoding task, i.e., possible nonlinearities in the ideal classification boundaries can indeed be safely ignored. Fig. 2f shows the decoding result of the WT ensemble of Fig. 2d using the linear classifiers. Despite the presence of Poisson noise, positions ($\tilde{y}$) decoded by reading the maternal morphogen values are always close to the ground truth positions (y). The root-mean-square-error (RMSE) is hardly larger than 1% (reminding that the morphogen noise level here is already comparable with the measured values), even smaller than the RMSE of a Bayesian decoder which allows arbitrary decision boundary geometry (Fig. S4a–c online).

2.3. The decoder quantitatively predicts phenotypes of morphogen mutants

We next demonstrate that such a decoder, whose overall geometry is solely determined by scaling, has a remarkable power to predict nearly all phenotypes of maternal morphogen mutants in

Drosophila, demonstrating it to be a satisfactory description of the actual gap gene system. Note that the values of (Bcd, mHb, and Tor) in mutants may lie outside of the WT region (but still nearby). In this case, we linearly extrapolate the classification planes (see Supplemental Text S5 online for justification of the extrapolation).

Fig. 3a–c shows the intersections of the linearly extrapolated classification planes with the bottom/left/back faces of the cube in Fig. 2d (marked by α, β, and γ, on which Tor = 0, Bcd = 0, and mHb = mHb_0, respectively), with the same color scheme as in Fig. 2. Maternal morphogen null mutants lie on these faces. For example, in the *nos*$^-$ mutant mHb is equal to mHb_0 throughout the entire embryo, corresponding to projecting the WT curve onto the γ plane. It is clear in Fig. 3c that along this projected *nos*$^-$ curve, domain iv is followed immediately by domain vii, indicating the loss of abdominal *kni* (v) and *gt* (vi) domains. This is exactly the case observed in experiments [43,55,56].

As another example, consider the *bcd*$^-$*tor*$^-$ mutant. mHb is now the only morphogen gradient, decreasing from its maximum value to zero from the anterior to the posterior pole. It is obvious in Fig. 3a, b that points on the mHb axis fall into the iv, v, and vi domains successively, corresponding to three gap gene domains *Kr*, *kni*, and *gt* appearing successively in this mutant embryo. As the Bcd = Tor = mHb = 0 point is classified into domain vi, the *gt* domain should extend all the way to the posterior pole. This is also the pattern observed experimentally [43,46].

More than predictions on the presence or absence of certain gap gene domains, a nearly continuous-valued fate map $\tilde{y}(y_{mut})$ can be constructed by incorporating all the 100 classification planes. That is, the 100 decision planes divide the morphogen space into 101 slices, corresponding to cell fates $\tilde{y}$ = 0% to 100% (see Supplemental Text S5 and Fig. S5 online for a detailed description of the procedure). In Fig. 3d, the predicted fate map for WT and 11 maternal morphogen mutants are shown as black curves. To see whether these predictions from scaling match experiments, we identify the peak and boundary positions for all gap gene domains (Table S1 online) from the published quantitative measurements of gap gene profiles in WT and various mutants [27,43,53,57,58]. For each of them, its position in mutant is plotted against its WT positions (yellow squares in Fig. 3d). Remarkably, predictions and experiments agree quantitatively in all cases.

Predicted fate map can also be converted to a predicted gap gene pattern. For y_{mut} in a mutant embryo, the gap gene expression level can be approximated by the composite function $G(\tilde{y}(y_{mut}))$, where *G* stands for the WT gap gene expression pattern, and $\tilde{y}(y_{mut})$ is the fate map. Two examples (solid lines) are shown in Fig. 4a, b. Measured profiles [43] are shown as dotted lines in lighter colors for comparison.

2.4. Decoder geometry constrains the structure of the underlying gene regulation network

Further analysis reveals interesting connections between the decoder structure and the underlying gene regulation. That is, the *Drosophila* gap gene network is structured in a way that enables scaling.

Consider the *tor*$^-$ mutant as an example. As dictated by scaling, the decision boundaries *Kr*–*kni*, *kni*–*gt*, and *gt*–*hb* should be inclined in the 3-d morphogen space, not perpendicular to the Bcd-mHb plane (Fig. 2e). This means that Tor should participate in positioning these boundaries to allow for scaling. Geometrically, when extrapolated to the Tor = 0 plane following these inclined classification planes, a cell fate in WT should appear at a more posterior position than if being orthogonally projected downward. Thereby in the *tor*$^-$ mutant, besides the fact that the posterior *hb*

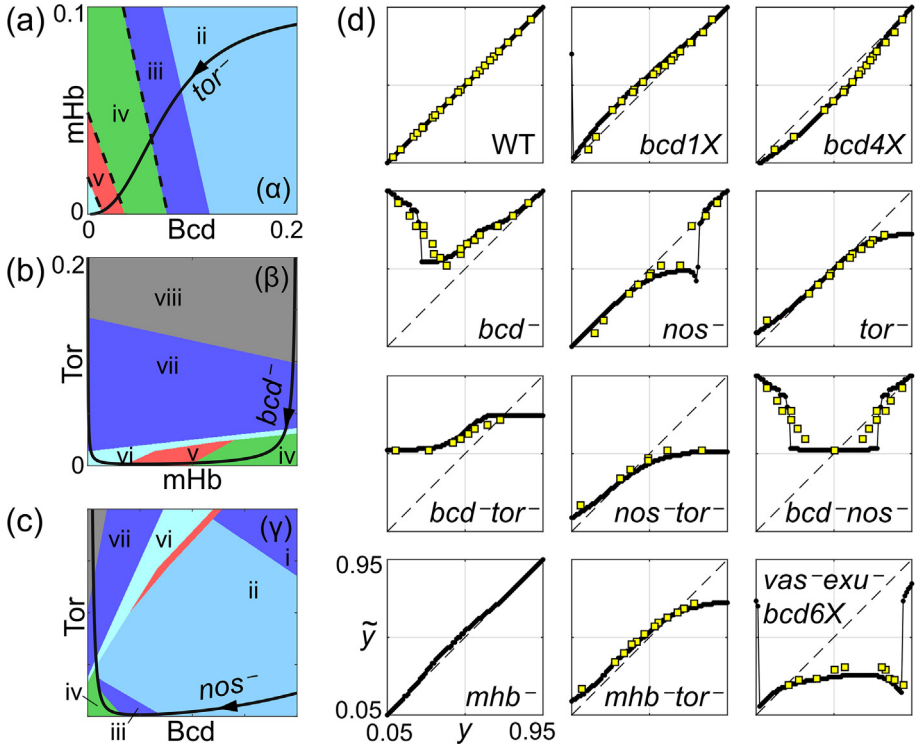

Fig. 3. Quantitative predictions on mutant fate maps by the phenomenological decoder. (a–c) The decoding results on the bottom/left/back faces (marked by α/β/γ) of the cube in Fig. 2d. Solid black curves are projections of the *L* = 1 WT curve onto these planes, which also represents the standard-sized mutant embryos *tor*$^-$/*bcd*$^-$/*nos*$^-$, respectively. The predicted gap gene expression in these mutants can be read out along these lines (arrowheads on them are pointing from head to tail). (d) Fate map $\tilde{y}(y)$ predicted for WT and another 11 different mutants (black lines) and the comparison with experimental measurements (yellow squares, cited from Refs. [27,43,53,57,58]). See Supplemental Text S6 and Fig. S6 (online) for discussion on the panels of *mhb*$^-$ and *vas*$^-$*exu*$^-$*bcd6X*.

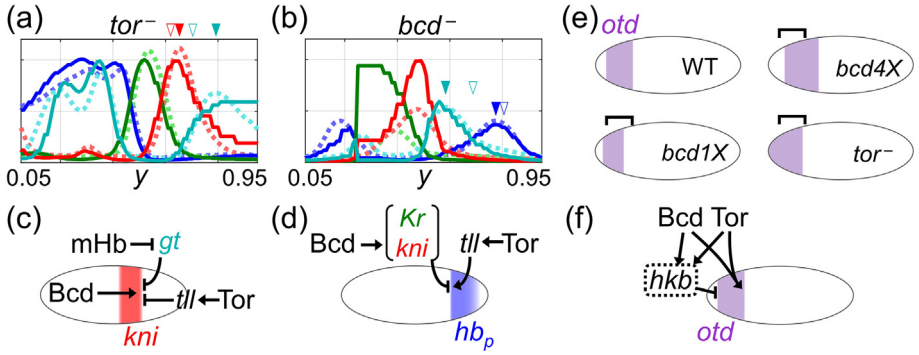

Fig. 4. The decoder reveals information about gene regulation logic. (a–b) The predicted gap gene patterns (solid lines) in *tor*$^{-}$ and *bcd*$^{-}$ are compared to that measured in Ref. [43] (dashed lines). The peak and boundary positions are correctly predicted. The peak position of the posterior *kni*, *hb*, and *gt* domains are marked by filled arrowheads, and their WT positions by the empty arrowheads. (c) "Redundant" regulation on the posterior boundary of *kni* domain as required by scaling. (d) According to the scaling decoder, the vi–vii boundary ($\tilde{y}$ = 0.75) is set by the balance between the opposing gradients Bcd and Tor. Biochemically, this is realized by indirect activation of Tor through *tll*, together with an indirect inhibition from Bcd, meditated by *Kr* and *kni*. (e) The predicted expression patterns of the head gap gene *otd*, which is completely consistent with experiments [64]. The structure of the decoder requires both Bcd and Tor to effectively activate *otd* for positioning its posterior boundary, while at the same time, both inhibit *otd* for defining its anterior boundary. (f) The regulations of *otd* proposed by experimentalists decades ago [64,65] is fully consistent with the logic deduced here.

domain disappears as a result of lacking the activation from *tailless* (*tll*) [59], the rest of the abdominal domains should also shift posteriorly. This prediction is fully consistent with experiments (Fig. 4a, where the filled and empty arrowheads mark the measured peak positions in *tor*$^{-}$ and WT, respectively).

This example may help us to understand the ubiquitous "redundant" regulations in the gap gene network. According to the simplest interpretation, mHb gradient defines the anterior boundary of the abdominal *gt* (vi) domain through inhibition; Gt inhibits *kni*, thereby setting the posterior boundary of *kni* (v) domain [46]. There is no "need", in principle, for Tor to be involved. But the observed shift of *kni* boundary in *tor*$^{-}$ clearly shows that in reality, Tor contributes (probably through *tll*) to the repression on *kni* [56,60,61], setting its posterior boundary together with mHb as well as Bcd [62]. We propose that such seemingly redundant regulations in fact tune the slope of *kni*-*gt* classification plane, so that it could align with the angle required by scaling (Fig. 4c). Scaling seems to be one important "goal" of such redundancy in the gap gene network.

Another example deals with the *bcd*$^{-}$ mutant (Fig. 4b). Bcd is well known to function in the anterior part. However, the region where Bcd plays a role seems to be much wider than naively expected—*bcd*$^{-}$ mutant affects even domain vi and vii near the posterior pole as shown by experiments. This aspect of Bcd should also contribute to tuning the decision boundary orientations to allow for scaling, as it has clearly been captured by our scaling-based decoder. To be more precise, according to our decoder the decision plane representing the *gt*–*hb* (vi–vii) boundary at $\tilde{y}$ = 0.75 is:

$$-0.85\mathrm{Bcd} - 0.12\mathrm{mHb} + 0.45\mathrm{Tor} = \mathrm{Const.}, \quad (7)$$

indicating that Tor should be effectively an activator for *hb* here while Bcd should play a repressive role (Fig. 4d). This speculation is consistent with the existing biological knowledge: Tor is known to activate the posterior *hb* domain through *tll* [60]. And the effective repression by Bcd is probably meditated by *Kr* and *kni*, upon whose mutation the posterior *hb* domain expands anteriorly [63].

A third example of this kind regards the head gap gene *orthodenticle* (*otd*), which is expressed between $\tilde{y}$ = 0.08 and 0.25 along the A–P axis. Position of the *otd* domain in mutants can be predicted straightforwardly by finding $\tilde{y}$ = 0.08 and 0.25 in the corresponding mutant fate maps (Fig. 4e). These predictions are again in agreement with experiments [64]: decreasing Bcd dosage shifts both the anterior and posterior *otd* boundaries anteriorly, while lacking Tor makes the *otd* domain fail to retract from the anterior pole, and shifts its posterior boundary slightly forward. These observations in mutants are directly related to underlying regulations (as in Ref. [65]), that Bcd and Tor both activate *otd* in defining its posterior boundary, while at the same time both repress *otd* (probably through *huckebein* (*hkb*)) in setting the anterior boundary (Fig. 4f). The gap gene regulation network seems to be organized in such a way to allow scaling.

2.5. Dissecting the contribution of each morphogen at each embryonic position

In our framework, scaling originates from the insensitivity of decoder output to the specific form of correlated fluctuations in local morphogen levels caused by length fluctuation. The forms of such correlated fluctuations are determined by the morphogen profiles (Eq. (6)). Therefore, if the morphogen profiles were perturbed, the alignment between the *y*-constant lines and the decoder's decision boundaries would be affected and scaling would be as least partially destroyed. To provide a quantitative test from this perspective, the influence of embryo length change in mutant embryos is studied. These fate-maps are obtained by substituting the morphogen profiles given by Eq. (6) (with $L \neq 1.0$) into the above constructed phenomenological decoder (Fig. 5a, c, d).

Nearly all the decision planes have non-negligible projections alone the Bcd axis according to the scaling decoder, implying that Bcd contributes to patterning throughout the entire embryo. Therefore, missing Bcd destroys scaling completely in the prediction—the gap gene pattern changes greatly with *L* (Fig. 5a). More specifically, with decreasing embryo length, the *bcd*$^{-}$ embryo is predicted to lose domain iv (*Kr*) and then v (*kni*). Amazingly, this phenomenon is observed in a recent experiment [25] (see Fig. S7c online for a detailed discussion).

Furthermore, increasing Bcd dosage also affects the matching between the decoder decision planes and the *y*-constant lines, predicting that in embryos with additional *bcd* copies, scaling should also be affected. Experimentally, the mid-embryo *hb* boundary is indeed reported to be unscaled in shortened embryos when Bcd dosage is increased [25] (Fig. 5b, red dots), which is accurately captured by our scaling decoder (Fig. 5b, black line. See also Supplemental Text S7 online for an analytical calculation).

In contrast to Bcd, at least some of the decision planes can have near-zero projection alone the mHb or Tor axis, implying that missing mHb or Tor affects scaling in only part of the embryo (Fig. 5c, d). The relative contribution to patterning from each of the three morphogens (i.e., projection of each decision plane along

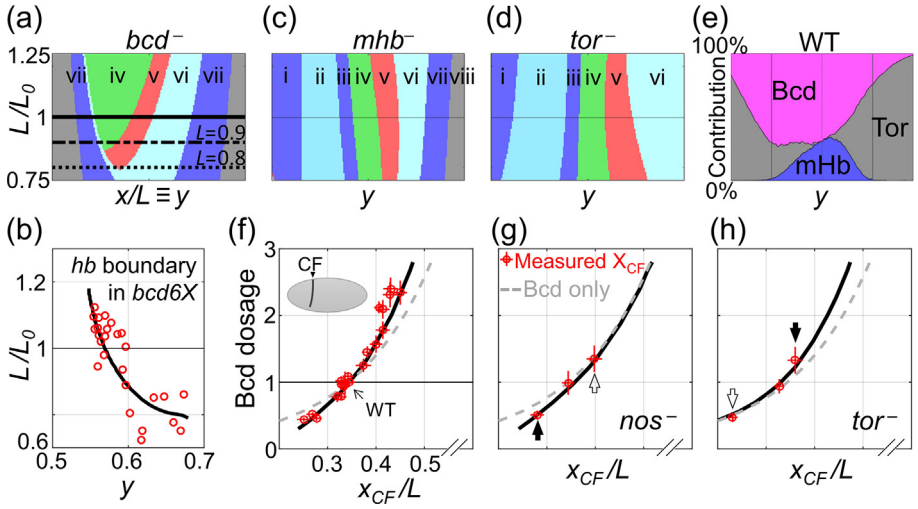

Fig. 5. Different morphogens collaborate to achieve scaling in different regions. (a) Missing Bcd destroys scaling throughout the embryo. In bcd^-, as L shrinks from 1.0 to 0.9 to 0.8 (solid, dashed, and dotted lines), the *Kr* (iv) and *kni* (v) domains are predicted to disappear successively, which is observed in experiments [25]. (b) The effect of increasing Bcd dosage on scaling is accurately captured by the scaling decoder. The position of predicted (black line) vs. measured (red circle for each individual embryo) [25] *hb* boundary (iii–iv boundary, $\bar{y}$ = 0.47) are shown. (c–d) In mhb^- and tor^-, scaling is affected mostly in the middle and near the two termini, respectively. (e) Relative contributions of the three morphogens to scaling across the embryo, as defined in Supplemental Text S8 (online). The horizontal axes of panels a, c, d, and e all range from 0.05 to 0.95. (f) The shift of cephalic furrow (CF) under Bcd dosage change. The solid line is our prediction and red dots with error bars (standard deviation) are from experiment data [53]. The dashed grey line shows the position of the same Bcd concentration as CF in WT. (g–h) The shift of CF position in nos^- and tor^- backgrounds, respectively. The observed shifts match our predictions (solid line) well. Axes and ranges are the same as in (f).

the three axes) across the embryo can be quantitatively defined (Supplemental Text S8 and Fig. S8a–c online) and is shown in Fig. 5e. Note that the morphogen mHb has long been considered dispensable or redundant, since losing mHb does not lead to any direct loss of the segment [47,48]. However, our results indicate that it in fact plays a crucial role in scaling in the abdominal region.

As a final example, we provide a quantitative explanation for the experimentally measured shift of the cephalic furrow (CF) under mutation of Nos or Tor plus Bcd dosage change, which has never been explained by previous models either. CF is the morphological boundary between head and thorax, located at y = 0.344 in WT. It is a morphological trait much downstream of the gap genes. But, as we believe that the scaling blueprint is established at the gap gene stage, we can regard CF as a hypothetical gap gene boundary at $\bar{y}$ = 0.344 and predict its position $y \equiv X_{CF}$ in various mutants. These predictions are compared with the measurements reported in [53] (Fig. 5f–h).

When Bcd dosage is perturbed, the predicted X_{CF} matches well with the experimental measurement (Fig. 5f). It is clear that X_{CF} shows certain robustness against Bcd dosage change—its shift is always visibly *smaller* than that of the iso-concentration point of Bcd (Fig. 5f–h, gray dashed line). Such robustness of boundary positions has long been noted, and is frequently attributed to some mysterious "self-correction" mechanism of the gap gene system [38,53,66]. In our framework, it is a direct reflection of the contributions of the other two morphogens.

Perhaps more convincing is the case when Bcd dosage is altered in the absence of mHb or Tor gradient. In nos^- mutant where mHb gradient is eliminated (Fig. 5g), with increasing Bcd dosage such robustness disappears, and X_{CF} follows the Bcd threshold exactly (marked by white arrow); while for decreasing Bcd dosage, such robustness still exists (black arrow). Similar but opposite phenomenon is seen in tor^- mutant (Fig. 5h). These phenomena are successfully captured by our model without any further tuning of parameters. Shift of CF in these cases can be easily understood from information provided in Fig. 5e—Bcd and Tor are the main contributing bi-gradient pair anterior to the CF, while the Bcd-mHb pair dominants the middle part behind CF. Therefore, the positional robustness of the CF against Bcd dosage change has different origins when shifted anteriorly or posteriorly. The same argument should apply to the shift of pair-rule stripes as well (Supplemental Text S9 and Fig. S9 online).

2.6. The scaling decoder can be implemented with gene regulation

The discussions so far are quite general, independent of any details in the decoder's biochemical implementation. In this section, we provide evidence that the scaling decoder can be implemented by gene regulation and more specifically by the known gap gene network.

First, consider a toy model with a static anterior morphogen B (like Bcd) with fixed length constant and a single gap gene H whose initial condition H_{init} serves as the second posterior gradient (like mHb) (Fig. 6a). The desired output is to have H being activated in the anterior half with the boundary located at y = 0.5 regardless of the embryo length L. This requires that the morphogen levels marked by the black dots or empty triangles (Fig. 6a) should both lie on the H boundary. Let the regulation network be that of the inset in Fig. 6b. From a dynamical perspective, this network is well known to have bi-stability and Fig. 6b shows a typical bifurcation diagram. Within the bistable range, the H-high/H-low states are separated by a critical line (red squares), which is the achieved decision boundary between the two cell fates. If the activation strengths are properly tuned, this critical line can be adjusted to have the same slope as that of the desired decision boundary in Fig. 6c. Such first-order approximation is already good enough for ±20% variations in embryo length. (Note that this is already a minimal but fully operational design, requiring only a toggle switch, for anyone who wishes to implement our proposed scaling mechanism using the synthetic biology approach.).

The gap gene network has more degrees of freedom and more scaling boundaries, and does not necessarily have to reach a dynamical attracting point. But the general idea is the same, that decision boundaries of the decoder correspond to boundaries between dynamical attracting basins. Based on the known gap gene network shown in Fig. 6d [45], we construct a differential

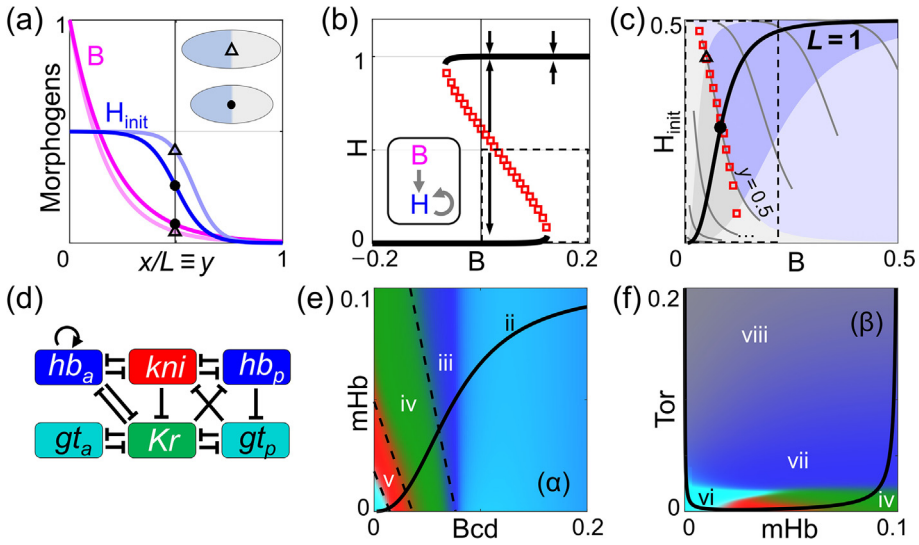

Fig. 6. The scaling decoder can be implemented by gene regulation network. (a) The profiles of two morphogens in a toy model are shown for two embryos of standard size (darker lines) and larger size (lighter lines). (b) The bifurcation diagram and the regulation network. A cell can reach one of the two bi-stable states depending on the values of the two morphogens, separated by the unstable manifold (red squares), which is the decision boundary separating the *H*-high and *H*-low fates. Its slope can be tuned by the activation strengths. (c) Within the realistic *L* range (± 20%, highlighted region), The $y = 0.5$ line is well approximated by the dynamical decision boundary in (b) (red squares). (d) The known gap gene network based on Ref. [45]. (e–f) The same plots as Fig. 3a–b, but implemented with an ODE model based on (d) (see Supplemental Text S10 and Fig. S10 online for details). Dashed black lines are decision boundaries of the phenomenological decoder, same as Fig. 3a.

equation model (see Supplemental Text S10 online for details). If fitted to the WT data [27] plus, importantly, the scaling requirement, the model can produce very similar decision boundaries as the phenomenological decoder (Fig. 6e, f), and hence correct predictions on mutants (which has not been achieved by gap gene network models previously, see Fig. S10 and Fig. S11 online for our results).

3. Discussion and conclusion

Scaling gene patterning can originate from local integrative decoding of non-scaling morphogen signals. In such a case, the effective input–output structure of the decoder is largely dictated by the requirement of scaling. Consequently, the underlying gene regulation system evolves to have its macroscopic behavior approximating the ideal decoder geometry. All the intricate biochemical details seem to be hidden and largely irrelevant.

We provided strong evidence that scaling in the *Drosophila* gap gene expression pattern indeed emerges in this way. There are quantitative agreements between the predictions from the scaling decoder geometry and the experiments on nearly all maternal morphogen mutants. We then showed that the scaling requirement also contains rich information about the overall gene regulation logic and the way the morphogen signals are being integrated, all these inferred properties are consistent with the existing knowledge of the gap gene regulation network. The decoder was further demonstrated to be implementable by dynamical gene regulation models.

We note that the concept of the optimal decoder (i.e., decoder structure determined by its function) is not new even within the *Drosophila* community [28,43]. Our contribution here is that we have provided a unified understanding of scaling, mutants' behavior, and gene regulation in the *Drosophila* gap gene system using an "optimal decoder". Importantly, we think that scaling is a central goal for the *Drosophila* decoder—as the morphogen profiles (e.g., Bcd) are already quite precise, their molecular noise should not be a major factor shaping the geometry of an optimal decoder. In Supplemental Text S11 (online) we demonstrate that a decoder optimally designed for correcting small and homogeneous morphogen noise is not optimal in the sense of scaling, nor does it explain the mutants' behavior as satisfactorily as the one starting from scaling.

Finally, opposing gradients exist in many different cases of development and regeneration [12,40,67]. Whether those opposing gradients are used to generate scaling pattern with our proposed mechanism can be explored by applying the same arguments in this paper—especially, trying to predict mutant patterns using a scaling-dictated phenomenological decoder. We think the same mechanism is very likely to be responsible for scaling along the A–P body axis in other long-germband insects, and in Supplemental Text S12 (online), we briefly discuss the situation of *Megaselia abdita* (another long-germband insect).

In this paper, we have bridged the gap between the *Drosophila* gap gene regulations and scaling. Patterns observed experimentally in maternal morphogen mutants have provided strong evidence that the gap gene network decodes the maternal signals in the way that a local decoder can give rise to scaling output. Many long-standing puzzles concerning the detailed pattern shifts in some double/triple mutants, "redundance" in gap gene network topology, quantitative gene regulation dynamics, etc., are addressed in a unified manner under this framework.

Conflict of interest

The authors declare that they have no conflict of interest.

Acknowledgments

This work was supported by the National Natural Science Foundation of China (12090053 and 32088101). We thank Timothy Saunders for providing data for Fig. S7b, d, and e (online).

Author contributions

Jingxiang Shen and Chao Tang conceived the project; Jingxiang Shen designed the study and performed the computational work;

Chao Tang and Feng Liu supervised the project; Jingxiang Shen and Chao Tang wrote the paper.

Appendix A. Supplementary materials

Supplementary materials to this article can be found online at https://doi.org/10.1016/j.scib.2022.06.014.

References

[1] Wolpert L. Positional information and the spatial pattern of cellular differentiation. J Theor Biol 1969;25:1–47.
[2] St. Johnston D, Nüsslein-Volhard C. The origin of pattern and polarity in the *Drosophila* embryo. Cell 1992;68:201–19.
[3] Gurdon JB, Bourillot PY. Morphogen gradient interpretation. Nature 2001;413:797–803.
[4] Crauk O, Dostatni N. Bicoid determines sharp and precise target gene expression in the *Drosophila* embryo. Curr Biol 2005;15:1888–98.
[5] Bier E, De Robertis EM. Bmp gradients: a paradigm for morphogen-mediated developmental patterning. Science 2015;348:aaa5838.
[6] Ghosh SM, Testa ND, Shingleton AW. Temperature-size rule is mediated by thermal plasticity of critical size in *Drosophila melanogaster*. Proc Biol Sci 2013;280:20130174–178.
[7] Klok CJ, Harrison JF. Atmospheric hypoxia limits selection for large body size in insects. PLoS ONE 2009;4:e3876.
[8] Briscoe J, Small S. Morphogen rules: design principles of gradient-mediated embryo patterning. Development 2015;142:3996–4009.
[9] Shilo BZ, Barkai N. Buffering global variability of morphogen gradients. Dev Cell 2017;40:429–38.
[10] Bollenbach T, Pantazis P, Kicheva A, et al. Precision of the Dpp gradient. Development 2008;135:1137–46.
[11] Almuedo-Castillo M, Blassle A, Morsdorf D, et al. Scale-invariant patterning by size-dependent inhibition of Nodal signalling. Nat Cell Biol 2018;20:1032–42.
[12] Čapek D, Müller P. Positional information and tissue scaling during development and regeneration. Development 2019;146.
[13] Holloway DM, Harrison LG, Kosman D, et al. Analysis of pattern precision shows that *Drosophila* segmentation develops substantial independence from gradients of maternal gene products. Dev Dyn 2006;235:2949–60.
[14] Lott SE, Kreitman M, Palsson A, et al. Canalization of segmentation and its evolution in *Drosophila*. Proc Natl Acad Sci U S A 2007;104:10926–31.
[15] Miles CM, Lott SE, Hendriks CL, et al. Artificial selection on egg size perturbs early pattern formation in *Drosophila melanogaster*. Evolution 2011;65:33–42.
[16] Ben-Zvi D, Shilo BZ, Fainsod A, et al. Scaling of the BMP activation gradient in *Xenopus* embryos. Nature 2008;453:1205–11.
[17] Ben-Zvi D, Barkai N. Scaling of morphogen gradients by an expansion-repression integral feedback control. Proc Natl Acad Sci U S A 2010;107:6924–9.
[18] Restrepo S, Basler K. Morphogen gradients: expand and repress. Curr Biol 2011;21:R815–7.
[19] Ben-Zvi D, Pyrowolakis G, Barkai N, et al. Expansion-repression mechanism for scaling the Dpp activation gradient in *Drosophila* wing imaginal discs. Curr Biol 2011;21:1391–6.
[20] Hamaratoglu F, de Lachapelle AM, Pyrowolakis G, et al. Dpp signaling activity requires pentagone to scale with tissue size in the growing *Drosophila* wing imaginal disc. PLoS Biol 2011;9:e1001182.
[21] Rahimi N, Averbukh I, Haskel-Ittah M, et al. A WntD-dependent integral feedback loop attenuates variability in *Drosophila* Toll signaling. Dev Cell 2016;36:401–14.
[22] Houchmandzadeh B, Wieschaus E, Leibler S. Establishment of developmental precision and proportions in the early *Drosophila* embryo. Nature 2002;415:798–802.
[23] Gregor T, Wieschaus E, McGregor AP, et al. Stability and nuclear dynamics of the Bicoid morphogen gradient. Cell 2007;130:141–52.
[24] Cheung D, Miles C, Kreitman M, et al. Scaling of the Bicoid morphogen gradient by a volume-dependent production rate. Development 2011;138:2741–9.
[25] Huang A, Rupprecht JF, Saunders TE. Embryonic geometry underlies phenotypic variation in decanalized conditions. Elife 2020;9.
[26] Wu H, Manu JR, et al. Temporal and spatial dynamics of scaling-specific features of a gene regulatory network in *Drosophila*. Nat Commun 2015;6:10031.
[27] Dubuis JO, Samanta R, Gregor T. Accurate measurements of dynamics and reproducibility in small genetic networks. Mol Syst Biol 2013;9:639.
[28] Dubuis JO, Tkačik G, Wieschaus E, et al. Positional information, in bits. Proc Natl Acad Sci U S A 2013;110:16301–8.
[29] Namba R, Pazdera TM, Cerrone RL, et al. *Drosophila* embryonic pattern repair: how embryos respond to *bicoid* dosage alteration. Development 1997;124:1393–403.
[30] Tanaka KM, Takahashi A, Fuse N, et al. A novel cell death gene acts to repair patterning defects in *Drosophila melanogaster*. Genetics 2014;197:739–42.
[31] Arya R, White K. Cell death in development: signaling pathways and core mechanisms. Semin Cell Dev Biol 2015;39:12–9.
[32] He F, Wen Y, Deng J, et al. Probing intrinsic properties of a robust morphogen gradient in *Drosophila*. Dev Cell 2008;15:558–67.
[33] He F, Wei C, Wu H, et al. Fundamental origins and limits for scaling a maternal morphogen gradient. Nat Commun 2015;6:6679.
[34] Bergmann S, Sandler O, Sberro H, et al. Pre-steady-state decoding of the bicoid morphogen gradient. PLoS Biol 2007;5:e46.
[35] de Lachapelle AM, Bergmann S. Precision and scaling in morphogen gradient read-out. Mol Syst Biol 2010;6:351.
[36] Manu SS, Spirov AV, et al. Canalization of gene expression in the *Drosophila* blastoderm by gap gene cross regulation. PLoS Biol 2009;7:e1000049.
[37] Vakulenko S, Manu RJ, et al. Size regulation in the segmentation of *Drosophila*: interacting interfaces between localized domains of gene expression ensure robust spatial patterning. Phys Rev Lett 2009;103.
[38] Houchmandzadeh B, Wieschaus E, Leibler S. Precise domain specification in the developing *Drosophila* embryo. Phys Rev E Stat Nonlin Soft Matter Phys 2005;72:061920.
[39] McHale P, Rappel WJ, Levine H. Embryonic pattern scaling achieved by oppositely directed morphogen gradients. Phys Biol 2006;3:107–20.
[40] Zagorski M, Tabata Y, Brandenberg N, et al. Decoding of position in the developing neural tube from antiparallel morphogen gradients. Science 2017;356:1379–83.
[41] Morishita Y, Iwasa Y. Accuracy of positional information provided by multiple morphogen gradients with correlated noise. Phys Rev E 2009;79:061905.
[42] Hironaka K, Morishita Y. Encoding and decoding of positional information in morphogen-dependent patterning. Curr Opin Genet Dev 2012;22:553–61.
[43] Petkova MD, Tkačik G, Bialek W, et al. Optimal decoding of cellular identities in a genetic network. Cell, 2019, 176: 844-855 e815.
[44] Tkačik G, Gregor T. The many bits of positional information. Development 2021;148.
[45] Jaeger J. The gap gene network. Cell Mol Life Sci 2011;68:243–74.
[46] Struhl G, Johnston P, Lawrence PA. Control of *Drosophila* body pattern by the Hunchback morphogen gradient. Cell 1992;69:237–49.
[47] Iish V, Lehmann R, Akam M. The *Drosophila* posterior-group gene *nanos* functions by repressing *hunchback* activity. Nature 1989;338:646–8.
[48] Hülskamp M, Schröder C, Pfeifle C, et al. Posterior segmentation of the *Drosophila* embryo in the absence of a maternal posterior organizer gene. Nature 1989;338:629–32.
[49] Struhl G. Differing strategies for organizing anterior and posterior body pattern in *Drosophila* embryos. Nature 1989;338:741–4.
[50] Furriols M, Casali A, Casanova J. Dissecting the mechanism of torso receptor activation. Mech Dev 1998;70:111–8.
[51] Johnson TK, Henstridge MA, Herr A, et al. Torso-like mediates extracellular accumulation of furin-cleaved Trunk to pattern the *Drosophila* embryo termini. Nat Commun 2015;6:8759.
[52] Poustelnikova E, Pisarev A, Blagov M, et al. A database for management of gene expression data in situ. Bioinformatics 2004;20:2212–21.
[53] Liu F, Morrison AH, Gregor T. Dynamic interpretation of maternal inputs by the *Drosophila* segmentation gene network. Proc Natl Acad Sci U S A 2013;110:6724–9.
[54] Gregor T, Tank DW, Wieschaus E, et al. Probing the limits to positional information. Cell 2007;130:153–64.
[55] Eldon ED, Pirrotta V. Interactions of the *Drosophila* gap gene *giant* with maternal and zygotic pattern-forming genes. Development 1991;111:367–78.
[56] Rothe M, Wimmer EA, Pankratz MJ, et al. Identical transacting factor requirement for *knirps* and *knirps-related* gene expression in the anterior but not in the posterior region of the *Drosophila* embryo. Mech Develop 1994;46:169–81.
[57] Wimmer EA, Cohen SM, Jäckle H, et al. *Buttonhead* does not contribute to a combinatorial code proposed for *Drosophila* head development. Development 1997;24:1509–17.
[58] Ochoa-Espinosa A, Yu D, Tsirigos A, et al. Anterior-posterior positional information in the absence of a strong Bcoid gradient. Proc Natl Acad Sci U S A 2009;106:3823–8.
[59] Kraut R, Levine M. Spatial regulation of the gap gene *giant* during *Drosophila* development. Development 1991;111:601–9.
[60] Bronner G, Jäckle H. Control and function of terminal gap gene activity in the posterior pole region of the *Drosophila* embryo. Mech Dev 1991;35:205–11.
[61] Pankratz MJ, Hoch M, Seifert E, et al. *Krüppel* requirement for *knirps* enhancement reflects overlapping gap gene activities in the *Drosophila* embryo. Nature 1989;341:337–40.
[62] Rivera-Pomar R, Lu X, Perrimon N, et al. Activation of posterior gap gene expression in the *Drosophila* blastoderm. Nature 1995;376:253–6.
[63] Surkova S, Golubkova E, Manu, et al. Quantitative dynamics and increased variability of segmentation gene expression in the *Drosophila Krüppel* and *knirps* mutants. Dev Biol 2013;376:99–112.
[64] Finkelstein R, Perrimon N. The *orthodenticle* gene is regulated by *bicoid* and *torso* and specifies *Drosophila* head development. Nature 1990;346:485–8.
[65] Gao Q, Wang Y, Finkelstein R. *othodenticle* regulation during embryonic head development in *Drosophila*. Mech Dev 1996;56:3–15.
[66] Driever W, Nüsslein-Volhard C. The bicoid protein determines position in the *Drosophila* embryo in a concentration-dependent manner. Cell 1988;54:95–104.
[67] Umesono Y, Tasaki J, Nishimura Y, et al. The molecular logic for planarian regeneration along the anterior-pcsterior axis. Nature 2013;500:73–6.

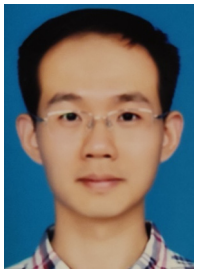

Jingxiang Shen is a postdoc researcher at the college of engineering, Peking University. He received his Ph.D. degree at Peking University in 2021. His research interest includes developmental biology, biophysics, statistical physics, inertial confinement fusion, and AI for science.

Chao Tang is a Chair Professor at School of Physics and the Director of Center for Quantitative Biology, Peking University. His research interest includes biological physics, systems biology, statistical physics, and complex systems.